Atmos. Chem. Phys., 3, 1267–1283, 2003
www.atmos-chem-phys.org/acp/3/1267/

Atmospheric Chemistry and Physics

Sensitivity studies of oxidative changes in the troposphere in 2100 using the GISS GCM

J. L. Grenfell[1, 2], **D. T. Shindell**[1], **and V. Grewe**[1, 3]

[1]NASA Goddard Institute for Space Studies and Center for Climate Systems Research, Columbia University, New York, USA
[2]Present address: Stratosphärengruppe, Institut für Meteorologie, Freie Universität Berlin, Germany
[3]Present address: DLR-Institut für Physik der Atmosphäre, DLR Oberpfaffenhofen, Germany

Received: 10 January 2003 – Published in Atmos. Chem. Phys. Discuss.: 1 April 2003
Revised: 23 June 2003 – Accepted: 8 July 2003 – Published: 3 September 2003

Abstract. We examine the relative importance of chemical precursor emissions affecting ozone (O_3) and hydroxyl (OH) for the year 2100. Runs were developed from the Comparison of Tropospheric Oxidants (Ox_Comp) modeling workshop year 2100 A2p emissions scenario, part of the Intergovernmental Panel on Climate Change (IPCC) third assessment report (TAR). While TAR examined only cumulative change, we examine individual components (NO_x, CH_4, CO, etc.). Also, since there will be climate changes in 2100 (not accounted for by TAR), we investigate the effect of changing our fixed SSTs/ocean ice from present day to 2100 conditions, as projected by a coupled ocean-atmosphere model with doubled CO_2. Unlike TAR we perform multiannual integrations and we include interactive lightning. Largest changes arose from the run with 2100 industrial NO_x (O_3=+16.9%, OH=+29.4% in July) and the run with 2100 methane (O_3=+17.4%, OH= $-$19.1% in July). In the latter run, large ozone increases in the NH upper troposphere appeared to repartition HO_2 into OH to such an extent that the lowering in OH associated with increased methane was overwhelmed in that region. Incorporating all changes collectively led to the July tropospheric ozone burden increasing from 426 to 601 Tg (+41.1%) and the July OH concentration increasing from 13.6 to 15.2×10^5 molecules/cm^3 (+11.8%).

1 Introduction

Accurately predicting oxidative and associated radiative changes occurring in the troposphere over the coming century is extremely difficult. The major oxidants ozone (O_3) and hydroxyl (OH) are not emitted directly into the atmosphere and their concentrations are determined by complex interplay between dynamics and chemistry which is a function of NO_x (defined here as [NO+NO_2+NO_3]), CO, H_2O and hydrocarbons. NO_x emissions from aircraft, lightning, soil and stratospheric input are subject to uncertainty. Model estimates of the impact of individual sources to the atmospheric NO_x concentration show even qualitatively a wide range (Grewe et al., 2001a). Ozone in the troposphere is formed from NO_2 in the presence of hydrocarbons and CO and is destroyed by dry deposition and chemical sinks. It has a short turnover time (days to weeks) and its concentration varies markedly with altitude near the tropopause, where radiative forcing sensitivities are largest . OH is formed by ozone photolysis in the presence of water vapor and is destroyed mainly by reaction with CO, NO_2 and CH_4 . It is the main chemical sink for methane and contributes, along with aqueous-phase chemistry to the oxidation of SO_2 into sulfate. Its local concentration can be measured with reasonable confidence (e.g. Poppe et al., 1994) and its global mean derived indirectly e.g. from methyl chloroform measurements (Prinn et al., 1995) but direct observations of its global distribution are lacking.

The model employed here has been extensively validated (Shindell et al., 2001) and was found to simulate present conditions satisfactorily. The model's greatest deficiency is an overestimate of the flux of ozone from the stratosphere to the troposphere due to the limited vertical resolution. Nonmethane hydrocarbons (NMHCs) are not directly included in our chemistry scheme although we do include a CO proxy for isoprene. Roelofs and Lelieveld, (2000) found that including NMHCs in a present-day simulation led to a 8% increase in O_3 and a 8% decrease in OH. Wang et al. (1998) found $<$15% more O_3 (mainly in the remote troposphere) and 20% less OH (mainly in NH summer). Trainer et al. (1993) concluded that O_3 is more often limited by NO_x rather than hydrocarbons.

There have been numerous recent model studies of future chemistry-climate interaction in the troposphere. Collins et

Correspondence to: J. L. Grenfell
(grenfell@strat01.met.fu-berlin.de)

al. (2000) simulated present-day and 2100 conditions with a CTM and found a 1.48 increase in the tropospheric ozone burden and a decrease by 0.79 in the turnover time. Stevenson et al. (2000) used a revised version of the same CTM and found a 1.32 and 1.49 increase in the ozone burden for runs with and without climate (defined here as temperature and humidity) change. Grewe et al. (2001b) simulated present day and 2015 conditions and noted the importance of coupling chemistry with precipitation changes, especially in the tropics. The Ox_Comp comparison (IPCC TAR, Sect. 4; Prather et al., 2003) compared projected (2100) O_3 and OH for fourteen models, including the GISS GCM. All produced comparable mean increases in the overall tropospheric O_3 burden but disagreed in the zonal mean. This was attributed mainly to differences in the transport schemes.

The response of the large-scale circulation to future climate change has been extensively investigated (Rind, 1998; Bengtsson et al., 1996; Ramstein et al., 1998; IPCC, 1996). Most models predict a weaker latitudinal gradient in surface temperature with associated weaker Hadley cell intensity, reduced surface winds, eddy transports and a smaller wavelength of maximum baroclinic instability. We present results for our model in Sect. 4. Section 2 provides a model description; Sect. 3 an overview of the runs; Sect. 4, results; Sect. 5, conclusions and future work.

2 Model description

A full description may be found in Hansen et al. (1983), Hansen et al. (1997) and Shindell et al. (2001). Briefly, we use a version of the Goddard Institute for Space Studies (GISS) general circulation model (GCM) having 72 longitudes and 46 latitudes ($\sim 4\times5^\circ$) horizontal resolution and 9 sigma levels in the vertical. The model used in this study has only a very limited stratosphere (two stratospheric levels with a dynamical lid at 10 hPa). Climatological (monthly) sea surface temperatures (SSTs) and ocean ice were fixed, so the model is not fully interactive.

The present day ocean (SSTs and ocean ice) was based on the AMIP (atmospheric modeling intercomparison project) 1979–1993 means. The "2100 ocean" (prescribed SST and ocean ice conditions) was taken from the last 20 years of a previous 50 year equilibrium integration of the GCM with doubled CO_2 and which used prescribed rates of ocean heat fluxes (the qflux scheme) (Hansen et al., 1983; Russell et al., 1985). A full analysis of this run is not the aim of this paper. It was used only as a tool to obtain an estimate of future climate conditions. Largest differences in (2100–2000) sea surface temperatures (SSTs) of 3–4° C occurred in far southern regions and in the north Atlantic. The global mean increase was 2.6° C. Incorporating 2100 ocean ice coverage led to a mean decrease in the global, annual mean from 4.38 (NH=4.28, SH=4.48) to 3.13 (NH=3.45, SH=2.81) kg ice/m^2.

Convection is calculated via adiabatic adjustment (Del Genio and Yao, 1993). We employ 9 chemical tracers using the "family" approach. There are 37 reactions for 24 molecules based on the Jet Propulsion Laboratory (JPL) 1997 kinetic data. No peroxy acetyl nitrate (PAN) or explicit NMHC chemistry is employed. The fastj photolysis scheme is used to calculate 14 photolysis reaction rates (Wild et al., 2000). The chemical timestep is 1 h whereas the dynamical timestep is 5 minutes. N_2O_5 hydrolysis (Dentener and Crutzen, 1993) on sulfate aerosol (Koch et al., 1999) is included. Wet and dry deposition are parametrized. An interactive cloud-lightning scheme is used to generate NO_x (Price et al., 1997). Emissions include NO_x (industrial, aircraft and soil) and CO (biomass burning, equivalent isoprene and industrial). Methane (CH_4) , carbon dioxide (CO_2) and nitrous oxide (N_2O) are set to prescribed values for each run. Ox burdens in the troposphere were calculated using an analysis technique based on the ozone mixing ratio, in which we defined the stratosphere as those gridboxes having greater than 150 ppbv ozone. This correlates reasonably well with the location of the meteorological tropopause, though the resolution in this region is not sufficient to simulate this well.

3 Overview of runs

We have performed present day (2000) and future (2100) simulations. Additionally, the relative simplicity of our chemical scheme enabled a large number (10) of sensitivity runs to be performed which quantified the effect of individual perturbations (Table 1), e.g. changing industrial NO_x, CO etc. All runs were ten years in duration (including a 2-year spin-up which was discarded). This expands upon the TAR studies in which models were run for only two years. All figures show eight year January and July average model output unless otherwise stated. The simulations were performed with a feedback of chemical species (O_3, CH_4) to the radiation so that changes in the chemical composition affected the dynamics (hence dynamical stability, cloud cover, lightning NO_x emissions, washout etc.) and vice-versa.

The Ox_Comp workshop examined the effect of future emissions by performing an intercomparison of model runs for the year 2100. Relative to the control run, the year 2100 run changed CH_4 from 1745 to 4300 ppbv; N_2O from 314 to 455 ppbv and CO_2 from 365 to 891 ppbv. For our control run, 1992 aircraft emissions data based on Baughcum et al. (1996) were scaled up by 37% (=4.6%/year) to reflect the increase from 1992 to 2000. For a review of the other GISS GCM source inventories used in the control run see Shindell et al. (2001).

The 2100 run was based on the IPCC A2 (IS92a) marker scenario for which emissions increased the most and population changed from six to fifteen billion. The projected emission data are more fully documented in the IPCC 2000 TAR Sect. 4. Rapid industrialized growth is assumed to

Table 1. Description of the ten runs with associated OH and ozone concentrations. OH values are global means (1×10^5 molecules cm^3) whereas ozone values represent total tropospheric burdens (Tg). Values in brackets for run one represent 95% confidence intervals. Runs eight and nine are stand-alone runs whereas all other runs combine to form run ten

Run	Description	OH (Jan)	OH (Jul)	Ozone (Jan)	Ozone (Jul)
1	Control (year 2000)	5.6 (0.1)	13.6 (0.2)	403 (5.2)	426 (5.0)
2	2100 industrial CO	5.1	13.0	407	426
3	2100 NO_x fossil fuel	7.4	17.6	471	502
4	2100 CH_4 = 4300 ppbv	4.6	11.0	464	500
5	2100 NMHCs	5.3	13.1	425	425
6	2100 ocean	6.1	14.8	412	420
7	2100 aircraft (1992*4.34)	5.7	14.0	406	426
8	Control but with 1.1CH_4	5.4	13.3	407	426
9	All 2100 changes except NO_x fossil fuel	4.7	11.4	490	513
10	All 2100 changes	6.1	15.2	574	601

occur over Asia (and parts of Africa) where emissions increase by ∼4% per year (Kato and Akimoto, 1992). CO and NO_x emissions over North America and Europe stabilize or decline slightly by 2100. Emissions of industrial NO_x were 108.9 Tg/year and of industrial CO were 2486 Tg/year. We also adopted the 2100 recommended Ox_Comp NO_x aircraft emissions of Baughcum et al. (1996) scaled up by a factor of 4.34. Parameterizing 2100 NMHCs was challenging since these compounds were not explicitly included in our chemistry scheme. Discussions within Ox_Comp suggested a doubling in the NMHC burden by 2100. After our runs were completed this factor was revised to 2.3 (TAR, p. 269; 150 to 350 Tg CO/year from 2000 to 2100) but we believe this does not greatly affect the results. As a sensitivity test, we chose to double CO emissions arising from isoprene (to 290 Tg CO/year). We used this approach because isoprene dominates the NMHC budget (TAR, p. 258, Table 4.7A) and its CO proxy was already present in our model. The 2100 NMHC distribution was also problematic. The introduction of agroforests in the tropics with associated fast-growing species favored by e.g. the rubber and timber industries suggests increased isoprene emissions whereas in other regions conversion to pasture land will tend to have the opposite effect; also, industrialization clearly favours emissions of anthropogenic rather than biogenic hydrocarbons. Climate change effects will also influence growing rates, speciation hence biogenic emissions. The overall effect is unclear (TAR 4.3.3). Ox_Comp chose not to recommend any particular future NMHC distribution. We therefore chose to retain our present-day isoprene distribution. Further details of the assumptions we make in deriving CO from isoprene emissions may be found in Shindell et al. (2001). The efficiency of conversion of isoprene into CO is uncertain, which should be bourne in mind when we discuss the HCHO response. In this paper we investigate the individual effect upon ozone and OH of each projected change for 2100 conditions (i.e. individual GHG, individual source inventory shift) relative to the year 2000 run. Table 1 summarizes the ten runs performed. Run 6 investigated the effect of changing from a present day to a 2100 ocean (SSTs and ocean ice) using output from a simple model of ocean heat storage (the qflux scheme) (further information is provided in Sect. 2) with doubled CO_2. Run 10 investigated the combined effect of all changes. We have also performed some stand-alone runs which were suggested (but not strictly required) for Ox_Comp. These included modifying the control with a 10% increase in methane (run 8) and a run having all 2100 changes except NO_x fossil fuel (run 9). The latter was intended to estimate amongst other things how well the oxidative capacity of the troposphere would fare without the positive influence of a projected NO_x increase (which tends to increase OH).

4 Results

Table 1 gives a brief description of the runs and shows January/July tropospheric O_3 and global OH concentrations for the ten runs. Table 2 shows 95% confidence intervals for ozone and hydroxyl (control run) in the lower, central and upper troposphere at low, mid and high latitudes. Table 3 shows global changes of chemical tracers in July for all runs. An important point to realise is, the runs performed here are complementary to the TAR report, and expand upon it in the ways discussed previously. Like the other models in TAR, the GISS model employs fixed SSTs. Naturally the model cannot therefore respond fully on the lower levels. This point should always be bourne in mind, especially where we discuss physical responses of the model e.g changes in the meridional circulation and cloudiness. There are numerous climate studies that also discuss the response of such phenomena, and which are not limited by the fixed SST constraint. It is the aim of this paper to complement and build-

Table 2. 95% confidence intervals in the control run in January and July for ozone (ppbv) and hydroxyl (1×10^5 molecules/cm^3) on model levels 1 (959 mb), 3 (787 mb) and 6 (323 mb) output on gridboxes close to the equator (2° N), mid latitudes (42° N) and the north pole

Month	Level	Equator	Ozone Mid-latitude	Pole	Equator	Hydroxyl Mid-latidude	Pole
	6	0.74	1.07	3.51	7.55	5.63	0.1
January	3	0.93	0.1	1.67	3.51	5.73	0.1
	1	0.1	0.1	3.55	6.68	4.83	0.1
	6	0.93	1.04	13.26	15.41	16.45	2.12
July	3	0.93	1.04	5.55	5.44	8.75	0.71
	1	0.1	0.93	0.93	10.31	13.85	2.62

Table 3. Global average July concentrations for chemical tracers in the GISS model. Concentrations are in pptv except CO which is in ppbv. For brevity, we show only July values (which generally featured a larger chemical response compared with January). The various sensitivity runs are explained in more detail in Table 1. The 95% confidence interval for the control run is shown in brackets

Run	NO_x	HNO_3	H_2O_2	CH_3OOH	HCHO	HNO_4	CO
Control	362 (0.9)	1616 (13.0)	1066 (17.9)	249 (2.1)	152 (2.1)	24.5 (0.5)	65 (1.1)
CO	363	1616	1178	251	148	26	78
NO_x	444	2200	993	223	211	29	63
CH_4	351	1635	1449	613	309	33	115
NMHC	362	1612	1153	250	148	25	75
Ocean	361	1646	1295	291	171	24	64
Aircraft	374	1673	1052	246	158	25	65
$1.1CH_4$	361	1617	1099	276	163	25	69
All-NO_x	355	1693	1970	721	346	34	137
All	446	2516	1840	667	487	44	131

upon the results of TAR; specifically we wished to test the effect of climate change upon our interactive chemistry (response of washout rates, effect of increasing temperature etc.) and compare it with the effect of emission changes, which is why we performed the run with projected 2100 SST data (run 6). Long-term runs with both interactive chemistry and a coupled ocean are desirable but are not currently tenable.

4.1 Control run

The tropospheric ozone burden (Table 1) was slightly different from a previously published (Shindell et al., 2001) value due to differing aircraft emissions. The model has been shown by those authors to reproduce well both the global distribution of ozone, with lower values in the Southern Hemisphere compared with the Northern Hemisphere, and the seasonal cycle for the present day atmosphere. The global OH concentration of 9.6×10^5 molecules/cm^3 agreed well with the value of 9.7×10^5 derived by Prinn et al. (1995) using CH_3CCl_3 measurements made between 1978 and 1994. OH values in this work are mass-weighted. Lawrence et al., (2001) note that when comparing OH values with the Prinn result, it is more appropriate to weight the values by the rate of reaction of OH with methyl chloroform; this may change the result by up to 30%. Table 4 shows our OH values for the 12 regions investigated by Lawrence et al. (2001). Our values compare well with the values shown in that work. Also, zonal mean height plots of ozone and OH for the control run (not shown) were found to be similar to other works (Hauglustaine et al., 1998; Mickley et al., 1999; Wang et al., 1998), except that we calculated ∼20% more ozone in NH summer. This results at least partially from excess influx from the stratosphere.

4.2 Run 2 (2100 industrial CO)

The tropospheric ozone burden increased only slightly (Table 1), and changes were small everywhere (Figs. 1a and b), which suggested that ozone production was mainly controlled by NO_x, rather than volatile organic compounds (VOCs) in the model. Of the other chemical tracers, only CO and H_2O_2 gave significant responses. CO increased by 50–100 ppbv mainly in the tropics on all tropospheric levels and decreased by 50–100 ppbv in NH mid-latitudes, consistent with the emissions scenario. H_2O_2 correspondingly increased by 500–800 pptv, again in the tropics and decreased by 100–150 pptv in NH mid-latitudes, as increased

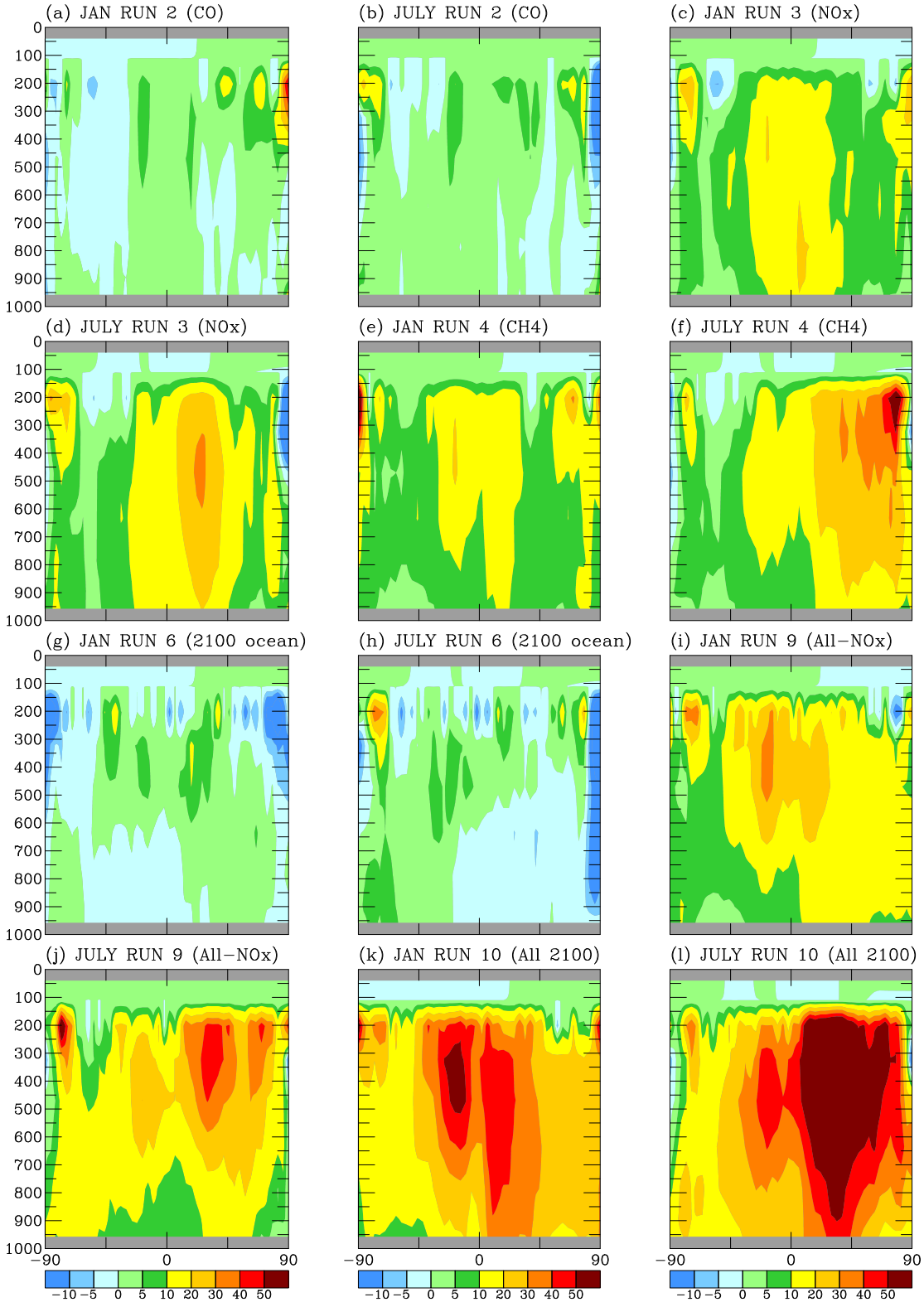

Fig. 1. Ozone change, (run x – control) (ppbv) in January and July for the CO, NO_x, CH_4, ocean, (all-NO_x) and all changes runs. The extremes of the color bar indicate all values less than −10 and greater than 50.

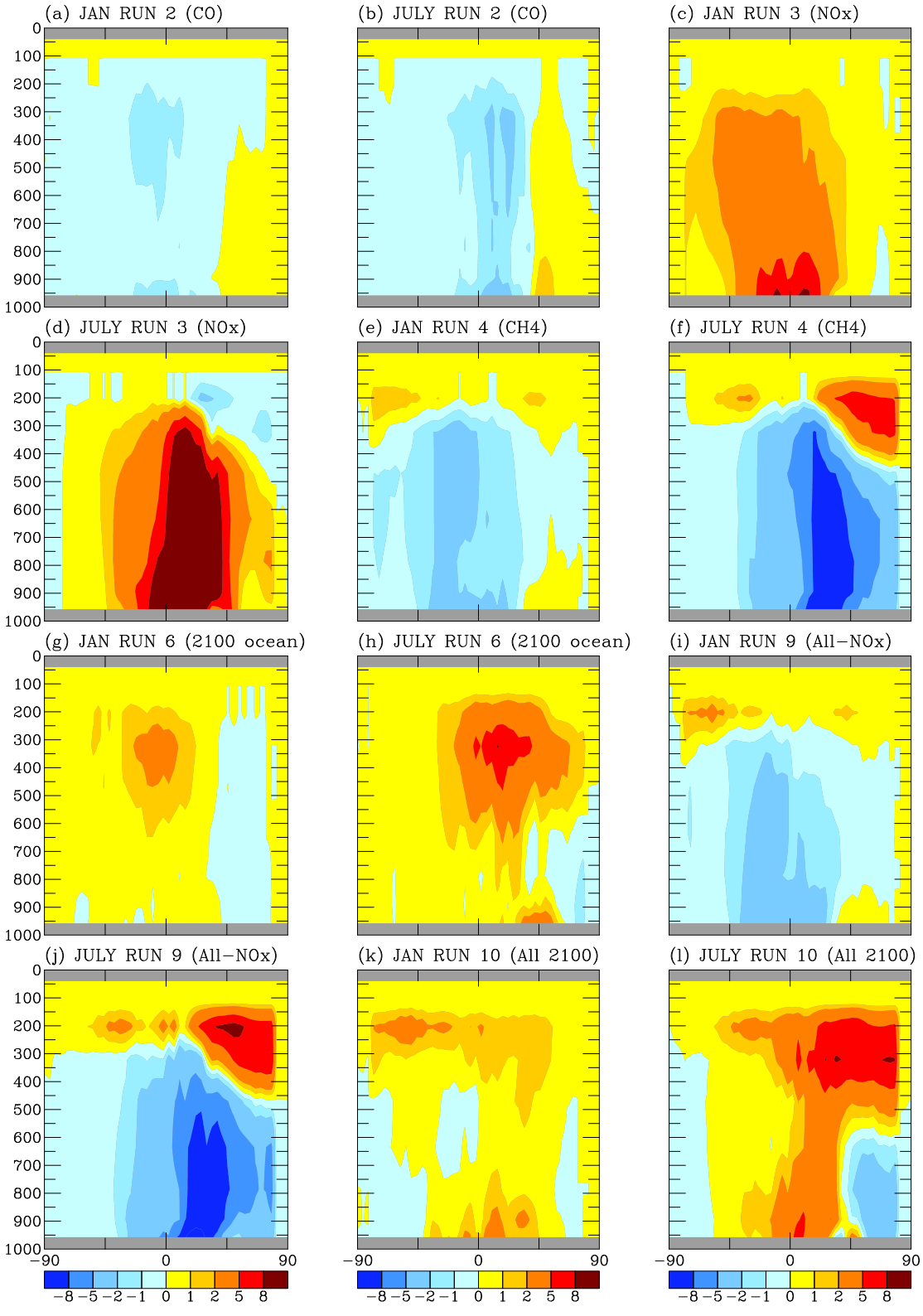

Fig. 2. Hydroxyl change, (run x – control) (1×10^4 molecules/cm^3) in January and July for the same runs as Fig. 1. The extremes ends of the color bar indicate all values beyond 8.

CO shifted the OH/HO_2 partitioning towards HO_2 increasing H_2O_2 formation and leading to reductions in OH in the tropics and increases at NH mid-latitudes (Figs. 2a and b).

4.3 Run 3 (2100 NO_x fossil fuel)

The tropospheric ozone burden increase was quite large (Table 1), constituting around 41% of the total increase in the best estimate of 2100 (2100 all changes run). Large increases in zonal mean ozone of 5–15 ppb in the SH and 10–30 ppb in the NH occurred over wide regions (Figs. 1c and d). All models in Ox_Comp produced largest absolute ozone increases in the upper troposphere, where photochemistry occurred more quickly, despite the fact that NO_x increases were larger on lower levels. The exact location of the ozone peak appeared to be sensitive to the transport scheme employed. Largest relative changes, however, did occur on lower levels in our runs. For the 2100 NO_x run, increases in OH of $5–15\times10^5$ molecules/cm^3 i.e. 20–60% occurred over wide regions (Figs. 2c and d) but mainly in the tropics. However, OH was lowered in NH summer in the upper troposphere at high latitudes. Usually, increased NO_x is associated with higher OH via $HO_2+NO\rightarrow OH+NO_2$ (reaction 1). A decrease in OH is more consistent with NO_x destroying OH via $OH+NO_2+M\rightarrow HNO_3+M$ (reaction 2). To test this we examined HNO_3 but results were inconclusive – it increased by relatively large (>1 ppb) values over much of the NH. A possible explanation for the lowered OH feature is that increasing ozone with altitude would favor a shift in the partitioning of HO_2 into OH and NO into NO_2. This would favor reaction 2 over reaction 1. Unfortunately the NO/NO_2 and OH/HO_2 diagnostics were not available for the runs discussed here, but the result has been illustrated by other modeling studies e.g. Hauglustaine et al. (1998) calculated a decrease by a factor five in HO_2/OH in NH summer from the ground up to 12 km. Removal of NO_x by conversion into HNO_3 followed by washout (reaction 1) is generally faster in the lower troposphere, which would appear to be inconsistent with the phenomenon occurring in the upper levels. Results suggest that the combined effect of the aforementioned altitude-dependant HO_x and NO_x partitioning responses more than compensate the washout effect. Grewe et al. (2001a) concluded that there may exist shortcomings in our chemistry in the upper troposphere, as typically seen in models (Jaegle et al., 1999) perhaps related to the use of Jet Propulsion Laboratory (JPL) 1997 reaction rates, as noted in Shindell et al. (2001). More work is required to explore this theme further.

For the other chemical tracers, NO_x increased over landmasses mainly in the tropics (500–1500 pptv) and decreased over NH landmasses (300–500 pptv), consistent with the emissions scenario. Largest increases occurred on the lower levels, although there was a secondary peak in the upper troposphere in mid-latitudes. This result, we believe, is sensitive to the model transport scheme. H_2O_2 correspondingly decreased (by 100–500 pptv) where NO_x increased. A significant source of H_2O_2 is the self-reaction of HO_2. NO_x increases tended to shift HO_2 into OH (the NO_x "see-saw" effect), consistent with the H_2O_2 decrease. CH_3OOH also decreased where NO_x increased, by 50–100 pptv. Again, this was because its main source involved HO_2, ($CH_3O_2+HO_2\rightarrow CH_3OOH$). HCHO increased by 200–400 pptv, mainly in the tropics on the lower levels. The increase tended to follow the landmasses i.e. occurred where NO_x was directly increased and was associated with enhanced NO_x-catalysed conversion of methane into HCHO in the model. HO_2NO_2 increased mainly in the upper troposphere, rather than on the lower levels, where NO_x increases were largest. This molecule was sensitive to temperature changes and readily underwent thermal decomposition. Results suggested that on the warmer, lower levels, the molecule is accordingly less sensitive to increases in NO_x. HNO_3 increased mainly over tropical landmasses, consistent with the emissions scenario. Interestingly, at the surface in NH mid-latitudes, despite NO_x decreases (due to lowered emissions), HNO_3 levels still increased (by several ppb). The HNO_3 lifetime was sufficiently long to enable travel over synoptic scales hence the NH mid-latitudes were influenced by the increased photochemical production occurring in the tropics.

Table 4. Regional OH in the control run (10^5 molec/cm^3)

Region	OH
below 800 hPa 90 S-30 S	3.6
below 800 hPa 30 S–0	11.1
below 800 hPa 0-30 N	15.9
below 800 hPa 30 N–90 N	11.4
800–500 hPa 90 S-30 S	3.9
800–500 hPa 30 S–0	9.8
800–500 hPa 0-30 N	15.2
800–500 hPa 30 N–90 N	11.0
500–300 hPa 90 S–30 S	3.9
500–300 hPa 30 S–0	11.2
500–300 hPa 0–30 N	15.0
500–300 hPa 30 N–90 N	8.7

4.4 Run 4 (2100 CH_4)

In this run the tropospheric ozone burden increases (Table 1) were comparable to the 2100 industrial NO_x run. Zonal mean ozone increased most in the NH upper troposphere in July (Fig. 1f). Zonal mean OH decreased in most regions. However, it actually increased in the upper troposphere during summer, where ozone increases peaked (Fig. 2f). It is well-known that increased ozone may lead to increased OH via O^1D+H_2O. Interestingly, HO_2NO_2 (which readily underwent thermal decomposition) increased by 100 pptv in the region of interest. Its only source in the model was via

Table 5. Chemical process budget in July showing a selection of tracers for run 1 (control), run 6 (2100 ocean) and run 10 (all 2100 changes). Values in brackets represent the 95% confidence interval for the control run. "Normalized" denotes values divided by the global mean species concentration in pptv. Wet deposition refers to large-scale (non-convective) rainout and washout

Units	Species	Process	Control	2100 ocean	All 2100
10^3 kg/s	O_3	Dry deposition	−38.3 (0.6)	−36.8	−59.9
10^3 kg/s	O_3	Chemistry	15.4 (0.7)	10.1	41.3
10^0 kg/s	NO_x	Dry deposition	−142 (3.7)	−137	−358
10^0 kg/s	NO_x	Chemistry	−1,199 (7.3)	−1,270	−3,417
10^0 kg/s	HNO_3	Moist convection	−1,104 (156.3)	−1,319	−3,245
10^0 kg/s*pptv	HNO_3	Moist convection Normalized	−0.683	−0.801	−1.290
10^0 kg/s	HNO_3	Dry deposition	−2,229 (67.9)	−2,289	−5,667
10^0 Kg/s	HNO_3	Wet deposition	−798 (57.2)	−867	−2,515
10^0 kg/s*pptv	HNO_3	Wet deposition Normalized	−0.494	−0.527	−1.00
10^0 kg/s	HNO_3	Chemistry	5,372 (33.1)	5,689	15,279
10^0 kg/s	H_2O_2	Moist convection	−5,784 (157.8)	−6,233	−6,411

(HO_2+NO_2+M); since temperature increased slightly, and since HO_2 decreased, this increase could only have arisen from an increase in NO_2. For the remaining chemical tracers, there occurred a large increase (several ppbv) of H_2O_2, mainly in the tropics. This change was the largest (0.5–1.0 ppbv) of all runs (except for the all changes run) – slightly larger than that of the 2100 ocean run and was associated with enhanced HO_x from methane oxidation. There was also a large (300–600 pptv) increase in HCHO, especially on the lower levels in the tropics. Again, this increase was larger than any other run (CH_4 increases, together with the increased NO_x run, contributed by far the bulk of the HCHO production).

4.5 Run 5 (increased CO for NMHC proxy)

In this run the tropospheric ozone burden increase was small (Table 1), similar to the 2100 industrial CO run. As already stated for that run, this demonstrated that ozone production was more often limited by NO_x, rather than VOC or CO availability.

4.6 Run 6 (2100 ocean), chemical response

Table 5 compares chemical processes for the control, the 2100 ocean run and the run with all changes. Table 6 is as for Table 5 but shows physical processes. The tropospheric ozone burden increased by 2.2% in January and decreased by 1.4% in July (Table 1). Other works have reported larger decreases on changing temperature and relative humidity. Johnson et al. (1999) found a 10% decrease in ozone in July under 2075 conditions. Brasseur et al. (1998) reported a 16.7% decrease in ozone in 2050 due to climate changes. Lower ozone was associated with the enhanced sink O^1D+H_2O and higher OH hence lower NO_x. We do in fact see a large reduction in the net chemical production of ozone (Table 5), though this is largely compensated for by reduced dry deposition and altered circulation.

Our zonal mean ozone (Figs. 1g and h) revealed moderate (1–5 ppbv) decreases on lower levels in the summer hemisphere, associated with enhanced water vapor. On upper levels there featured moderate increases (5–10 ppb) associated with increased NO_x from lightning. Other studies have incorporated fixed lightning, hence overlooked this potential source of ozone, which accounted for some (but probably not all) of our discrepancy with other studies. Grewe et al. (2001b) compared 1990 and 2015 and found that a decrease of precipitation in the tropics led to slower washout hence increased NO_x of the order 10% in their model. They also found that cloudwater changes could impact HNO_3 washout, hence affect NO_x. In our runs, precipitation also decreased, mainly over the Indian subcontinent (see Sect. 4.6.1) but we found little correlation between cloudwater and NO_x changes. There were however some similarities in the ozone and cloud responses (see Sect. 4.6.1). The O^1D+H_2O sink may be affected by changes in clouds which impact O^1D via scattering. Future work should examine this further. Finally, Table 5 revealed a 4% global decrease in dry deposition (an important sink) of ozone for the 2100 ocean run compared with the control. This arose chiefly due to reductions in sea-ice (some regions, e.g. Hudson Bay, McMurdo Bay suffered up to 50% loss). Other studies have incorporated fixed sea-ice hence have overlooked this potential "source" of ozone.

Our global OH change (Table 1) compared reasonably well with other studies – Brasseur et al. (1998) reported a 7% annual increase whereas Johnson et al. (1999) reported a 14% (July) increase in OH associated with temperature and

Table 5. Continued

Units	Species	Process	Control	2100 ocean	All 2100
10^0 kg/s*pptv	H_2O_2	Moist convection Normalized	−5.43	−4.81	−3.48
10^0 kg/s	H_2O_2	Dry deposition	−2,965 (89.0)	−3,421	−3,953
10^0 kg/s	H_2O_2	Wet deposition	−1,073 (36.0)	−1,431	−1,636
10^0 kg/s*pptv	H_2O_2	Wet deposition Normalized	−1.007	−1.105	−0.889
10^0 kg/s	H_2O_2	Chemistry	11,811 (273.7)	13,161	14,736
10^0 kg/s	CH_3OOH	Dry deposition	−771.0 (9.2)	−853	−1,622.4
10^0 kg/s	CH_3OOH	Chemistry	791.0 (41.0)	899	1,771.9
10^{-1} kg/s	HCHO	Dry deposition	−4,633 (93.2)	−4,924	−13,288
10^{-1} kg/s	HCHO	Wet deposition	−404.1 (54.2)	−498	−1,428.9
10^{-1} kg/s*pptv	HCHO	Wet deposition Normalized	−2.659	−2.912	−2.934
10^{-1} kg/s	HCHO	Moist convection	112.3 (102.7)	84.7	727.5
10^{-1} kg/s*pptv	HCHO	Moist convection Normalized	0.747	0.496	1.493
10^{-1} kg/s	HCHO	Chemistry	6,046 (168.3)	6,527	17,825
10^0 kg/s	HO_2NO_2	Chemistry	−3.8 (4.6)	−5.3	+12.3
10^2 kg/s	CO	Chemistry	−342.5 (7.4)	−332	−414.0

Table 6. Physical parameters in the model in January for the control run, changed ocean run and all 2100 changes run. All values are global mean. Values in brackets represent the 95% confidence interval for the control run

	Run 1 (control)	Run 6 (2100 ocean)	Run 10 (All 2100)
Surface Temperature (° C)	11.87 (0.15)	15.11	15.67
Supersaturated cloud (%)	42.78 (0.54)	43.61	42.87
Convective cloud (%)	9.99 (0.26)	8.88	9.07
Precipitation (mm/day)	3.06 (0.05)	2.97	3.18
Evaporation (mm/day)	3.07 (0.07)	2.98	3.19
Water column (mm)	21.26 (0.13)	27.25	27.55
Ocean ice (%) (fixed)	3.73 (0.00)	2.64	2.64
Snow cover (%)	14.72 (0.30)	12.64	12.17
d(T)/d(latitude)	−3.15 (1.53)	−2.90	−2.98
Tropospheric static stability	4.77 (0.03)	4.91	4.88

humidity increases under doubled CO_2 conditions. More recently, Johnson et al. (2001) report OH changes of −4 to +19% depending upon location and season. Zonal mean OH (Figs. 2g and h) increased by 2–7×10^5 molecules/cm^3 i.e. 10–35% compared with the control run, mainly in the tropical upper troposphere and centered at about 20 N in January moving to 20 S in July, associated with the seasonal shift of the inter-tropical convergence zone. The high altitude of the peak (despite higher increases in H_2O at lower levels, not shown) reflected uv availability.

Regarding other chemical tracers in the model, H_2O_2 increased by 1–2 ppbv, and CH_3OOH by 50–150 pptv, both mainly in the tropics, associated with water vapor (hence HO_x) increases, and similar to the responses for the increased methane run. Table 5 shows faster removal of the soluble gases due to wet deposition and convection for the 2100 ocean run. To isolate the cloud effect we also show values normalized by concentration. Results implied a general increase in both wet deposition and moist convection of 5–10% due to this effect (e.g. wet deposition of HNO_3 changed from −0.494 to −0.527). The exception was the moist convective removal of H_2O_2, which actually decreased; unlike HNO_3, this specie was most abundant in the tropics, where convective clouds decreased slightly (Table 6).

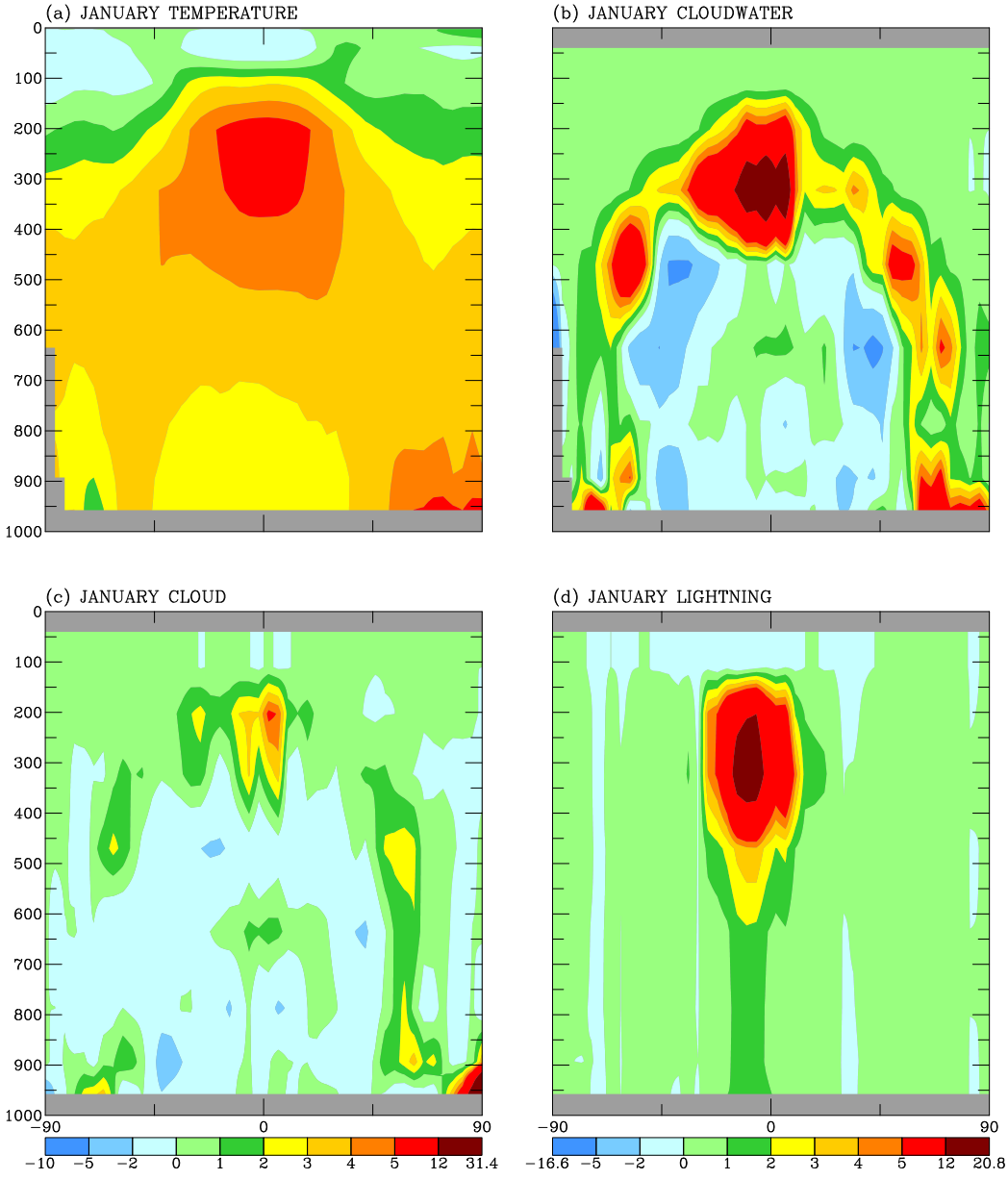

Fig. 3. (2100 ocean – control) in January **(a)** temperature (K), **(b)** cloudwater (ppmm), **(c)** total cloud cover (%) and **(d)** NO_x from lightning (1×10^{-2} kg/s).

4.6.1 Physical response

Figures 3a–d show changes in zonal mean temperature (° C), cloudwater (1×10^{-6} kg/kg), total cloud (%) and production of NO_x from lightning (1×10^{-2} kg NO_x/s) for the 2100 ocean run in January (i.e. during the large NH surface warming). Figures 4a–d show a latitude-longitude projection of changes in surface temperature (° C), precipitation (mm/day), total cloud (%) and lightning (flashes/minute).

Precipitation: This quantity decreased 2.9% in the global mean (Table 6). The decrease occurred most strongly (10–20 mm/day) over the ocean near the Indian peninsula (Fig. 4b) for this, and other runs with modified oceans, both in winter and summer. Curiously, the model calculated a general increase in the land-sea temperature contrast, which would argue for a stronger Asian monsoon with heavier precipitation. The model sometimes had problems in capturing mesoscale dynamics, especially over peninsulas and islands, due to its rather coarse horizontal resolution, so may not be the best tool to simulate the Monsoon. Many factors influence the Monsoon response – it is beyond the scope of this paper to enter into a discussion of them all.

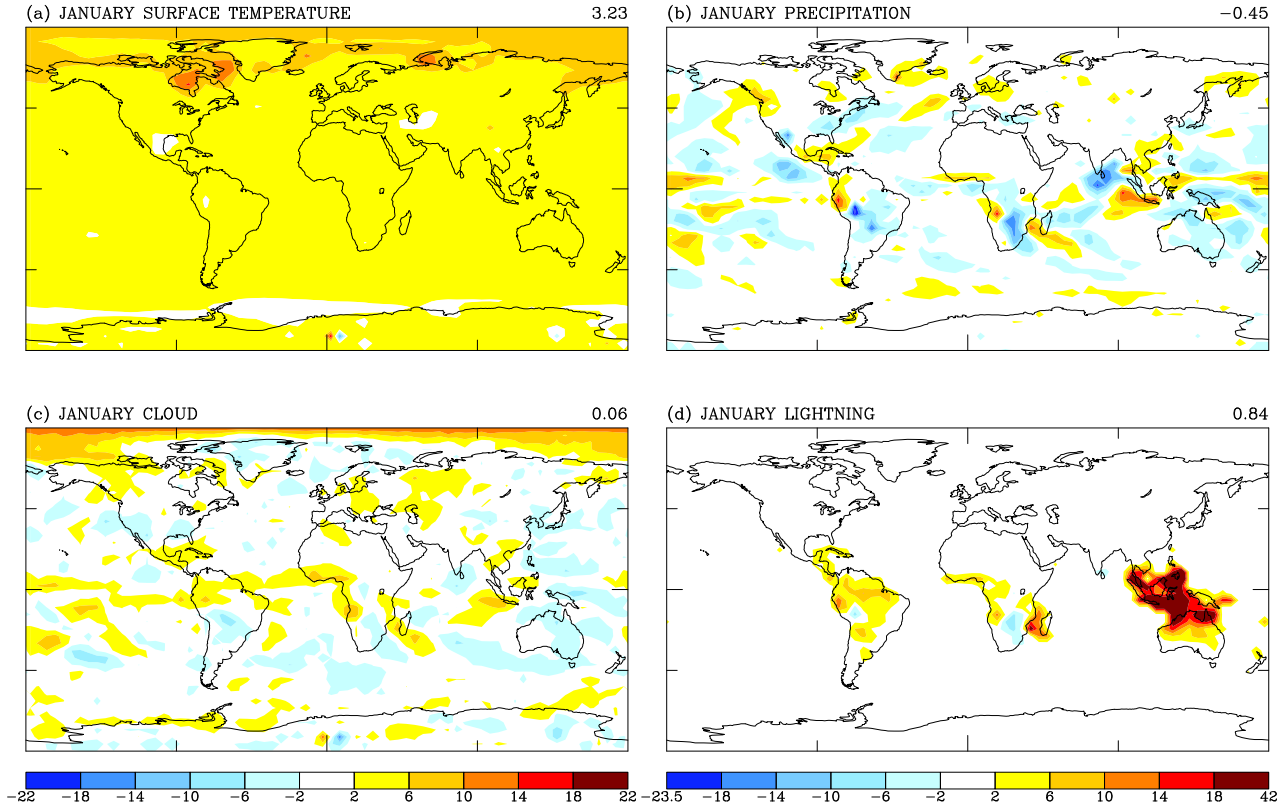

Fig. 4. (2100 ocean – control) in January **(a)** surface temperature (K), **(b)** precipitation (mm/day), **(c)** total cloud in column (%) and **(d)** total lightning in column (flashes/minute); precipitation has been multiplied by 5, cloud by 0.5, lightning by 5×10^{-4}.

Temperature (and clouds): The mean surface temperature increased from 11.87° C in the control run to 15.12° C in the 2100 ocean run (Table 6). Large, wintertime warming (5–10 K) extended from 45 to 90° in both hemispheres (Figs. 3a and 4a). Interestingly, the response in the run with all 2100 changes tended to be higher than the linear sum of the individual runs which suggested some non-linear feedback process in operation. The supersaturated clouds were enhanced mainly in the lower troposphere where they may effectively trap outgoing thermal radiation (increasing the radiative forcing there by 10–20 W/m^2) and lead to surface warming. The latitude-longitude plots (Figs. 4a and c) however, showed that although there was some correlation between increased clouds and increased surface temperatures in NH mid-high latitude winter, this was not always the case. For example, Hudson Bay warmed massively, but showed only a small cloud increase. On inspecting the sea-ice change (not shown) it was clear that areas such as this suffered large decreases in albedo due to lowered sea-ice, which decreased by 29.2% in the global mean (Table 6). Lowered surface albedo tended to increase surface warming directly.

Lightning (and clouds): Figs. 3d and 4d revealed largest lightning increases in the tropical upper troposphere, especially over Micronesia and the Amazon Basin. NO_x from lightning (Table 5) increased globally from 4.89 TgN/year in the control run to 6.86 TgN/year for the 2100 ocean run. Given this result, it was at first puzzling that total convective cloud cover should decrease to such an extent (Table 6). The explanation lay in increased deep convective frequencies. Decreased shallow convective cover and frequency led to an overall decrease in total convective cloud cover. Decreased convective cloud cover over wider scales was associated with weakened Hadley overturning in the tropics and occurred despite water vapor increases. Supersaturated cloud cover (and water vapor) tended however to increase (except for run 9, i.e. all changes except NO_x fossil fuel). It appeared therefore to be more sensitive to water vapor increases and less sensitive to the weakening in vertical overturning. Supersaturated clouds are more important regulators of climate (Del Genio et al., 1996; Poetzsch-Heffter et al., 1995) due to greater coverage and longer lifetimes compared with convective clouds. In ppbv NOx the lightning increases corresponded to +5.8% (202 hPa), +3.2% (322 hPa) and +1.5% (470 hPa).

4.7 Run 7 (2100 aircraft)

Interestingly, the total tropospheric ozone burden (Table 1) did not change appreciably. Increases of 10–20% occurred in the NH but these were offset by smaller decreases which occurred throughout the SH (not shown). The SH signal was only of low significance (1–2 sigma). Global mean OH increased by 1.8% in January and 2.9% in July. Zonal mean OH increased everywhere except in the upper troposphere at high latitudes similar to the 2100 fossil fuel emissions as already discussed in Sect. 4.3.

Regarding the other chemical tracers, NO_x increased mainly in the NH mid-latitude upper troposphere by 50–100 pptv in January and 100–200 pptv in July. There was a smaller ($\sim$50 pptv) peak at the surface immediately below. HO_2NO_2 also increased in the NH upper troposphere, by 25–50 pptv, comparable to the run with 2100 industrial NO_x (run 3). HNO_3 increased by 100–200 pptv throughout the NH mid-latitude troposphere. Remaining tracers showed only small responses.

4.8 Run 8 (2100 1.1*CH_4)

This, together with the "all changes except NO_x" run were both stand-alone runs, whereas the other runs all combined to produce run 10 (the all 2100 changes run). Run 8 was performed by Ox_Comp to investigate the sensitivity of present day OH to a prescribed (10%) increase in methane. The tropospheric ozone burden (Table 1) did not change appreciably. Global mean OH decreased by 3.6% in January and 2.2% in July (annual mean, 2.9% decrease). This compared reasonably well with other Ox_Comp models, who reported (annual) decreases in the range 2.9–3.5% (IPCC, 2001).

4.9 Run 9 (All 2100 changes except NO_x)

The rationale here was to investigate the response of OH without the positive influence of a future NO_x increase. Global mean OH decreased by 16.1% in January and 16.2% in July (Table 1). This result differed from the other four Ox_Comp models who performed this scenario. They reported a 41%, 39%, 37% and 43% decrease (mean=$-$40%). Some of the discrepancy arose because, unlike the other models, we changed the SSTs. This counteracted the decrease in OH (from increased VOCs) by increasing the water vapor.

4.10 Run 10 (All 2100 changes)

In this run the tropospheric ozone burden increased by 42.4% in January and 41.1% in July (Table 1), corresponding to a mean increase of 15.8 DU throughout the troposphere. This compared very well with the Ox_Comp results which were in the range 14.7 to 16.5 DU (TAR, Table 4.11; using 1 DU=10.94 Tg). Figures 1k and l, which show the zonal mean absolute change in ozone, revealed large (40–50 ppbv) surface increases in NH mid-latitudes and even larger (40–80 ppbv) increases in the upper troposphere in tropical to mid-latitude regions. Compared with run 9 (all changes except NO_x), approximately half this ozone increase was attributable to increased NO_x from fossil fuel. The GISS model produced a rather large July maximum at around 300 mb in the NH extra-tropics comparable to the UCI model and MOZART2 (see TAR, Fig. 4.12) but calculated smaller increases in other regions. Differing zonal mean behavior between Ox_Comp models was attributed by TAR mainly to differences in the model transport schemes. Our model differed in that we changed the SSTs (hence increased the water vapour), and did not explicitly include NMHCs. These two factors suggest decreased ozone in our model. On the other hand, we included online clouds, calculated an increase in NO_x due to lightning, and decreased ozone dry deposition via decreased ocean ice. These factors suggest increased ozone. The overall result has placed us well within the range quoted by the other Ox_Comp models.

Our global mean OH change (Table 1) was quite different from the other Ox_Comp models, who reported an annual mean decrease in the range 6 to 25% (mean 16%). However, as already mentioned, we changed the SSTs, which led to increased OH via increased water vapor. There have been several recent modeling studies of future climate change who also changed the SSTs, and who reported increased OH. Our results were rather higher than those studies. For example, Brasseur et al. (1998) reported a 2.2% annual increase in OH due to the combined effect of anthropogenic emissions and changes in temperature and relative humidity. However, those authors employed NO_x increases only up to 2075, and did not use the highest emissions scenario. Johnson et al. (1999) similarly reported -2 to +4% change depending on season but they employed NO_x changes only until 2050 and also did not use the highest emissions scenario. The percentage changes in industrial NO_x were: present work=(79%); Brasseur et al. (1998)=55%; Johnson et al. (1999)=73% . Also, our model produced more NO_x due to lightning. Finally, there featured increased OH in NH summer in our model which we believe was related to increased ozone in this region (see Sect. 4.4). Zonal mean OH (Figs. 2k and l) nicely revealed the opposing influences of the various individual runs. For example. it increased in the tropics at the ground (due to the 2100 industrial NO_x run ; Figs. 2c and d), in the upper troposphere (due to the changed ocean, Figs. 2g and h) and in the extratropics on the upper levels (due to the ozone effect arising from increasing the methane, already discussed) whereas it decreased in mid to high latitudes in both hemispheres, due to increased industrial CO, methane and NMHCs (e.g. Figs. 2a, b, e, and f).

Regarding the remaining chemical tracers, NO_x increased by 1–2 ppbv mainly in the tropics and on the lower levels (consistent with the industrial emissions scenario) but also featured a secondary peak (up to 200 ppt) in the NH extra tropics associated with increased lightning and aircraft

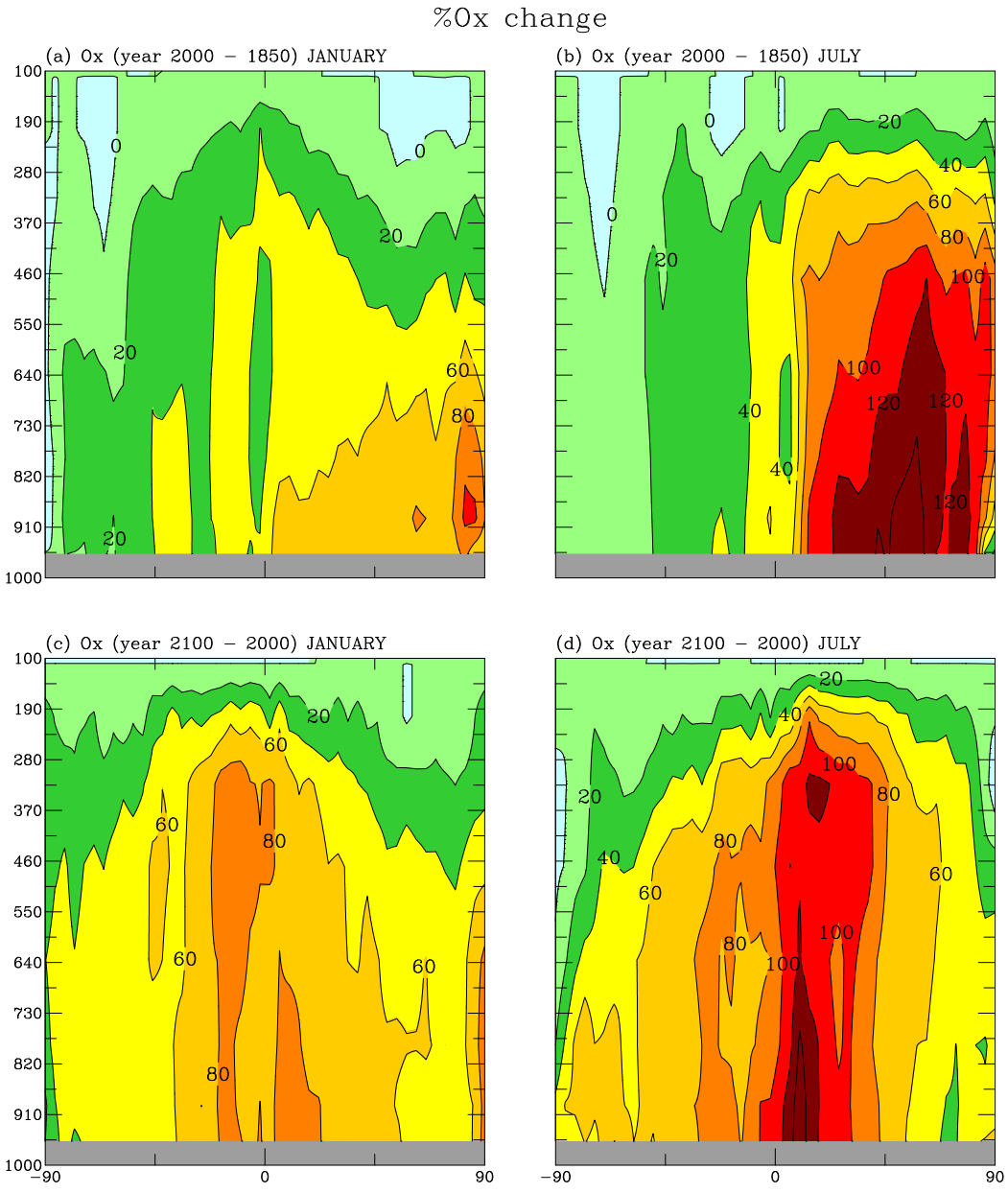

Fig. 5. %Ozone change in **(a)** January, **(b)** July, 1850 to 2000; **(c)** January, **(d)** July for the all changes run – control run.

emissions. It decreased by 300–400 pptv in the NH upper troposphere associated with the anomalous increased OH from the increased CH_4 (see Sect. 4.4 for further details). In the tropics, H_2O_2 increased on all levels by 2–3 ppbv, as did CH_3OOH by 500–1000 pptv; both effects arose mainly from (in order of importance) the changed CH_4 and ocean runs. HO_2NO_2 increased on the upper levels (but not the lower levels, see Sect. 4.3) by 50–200 pptv, associated with (in order of importance) the CH_4, industrial NO_x and aircraft runs. HCHO increased by 1–2 ppbv mainly in the tropics on the lower levels, associated mainly with the changed CH_4 and industrial NO_x runs. CO increased by 50–100 ppbv, mainly in the tropics and decreased by 20–25 ppbv over Europe and North America (due to decreasing emissions); the tropical increase was associated mainly with (in order of importance) the changed CH_4 and CO industrial runs.

A central question which coupled chemistry-climate models may address is the change in downward fluxes of ozone and NO_x from the stratosphere to the troposphere. As mentioned in Sect. 2, the model used in the present study has a very limited stratosphere, although future work will include a more realistic stratosphere to enable us to better understand

Table 7. Changes in Ox (10^3 Kg/s) and NO_x (Kg/s) over the tropospheric column in July arising from (1) vertical advection and (2) chemistry for the control (run 1), 2100 ocean (run 6) and all 2100 changes (run 10). Data has been averaged over the latitude bands 2–26 N (a region of overall ascent) and 34–42 N (a region of overall descent). Values in brackets represent the 95% confidence interval for the control run

	Ozone (2–26 N)	Ozone (34–42 N)	NO_x (2–26 N)	NO_x (34–42 N)
Control (run 1)				
advection	−18 (3.5)	11 (3.7)	−22 (1.7)	1 (2.4)
chemistry	−0.1 (0.1)	4.2 (0.1)	−147 (3.3)	−236 (4.9)
2100 Ocean (run 8)				
advection	−19	11	−27	1
chemistry	−1.4	3.9	−162	−247
All 2100 (run 10)				
advection	−48	11	−137	29
chemistry	4.3	7.8	−661	−469

the effects of climate on stratospheric-tropospheric exchange (STE). We have nevertheless calculated a first-order estimate of STE processes (Table 7). In our model, NO_x and ozone were fixed, and proportional to each other in the stratosphere. Table 7 shows Ox and NO_x changes in July due to vertical advection and chemistry averaged over the tropospheric column and across latitude band 2–26 N (a region of overall ascent) and 34–42 N (a region of overall descent) for the control run, the 2100 ocean run and the 2100 all changes run. For the 2100 ocean run Ox advective changes were not significant compared with the variability of the control run. The chemistry changes were, however significant for this run and led to a lowering in Ox consistent with the reaction O^1D+H_2O, as explained previously. The advection diagnostic reflected changes in (a) the large-scale meridional circulation and (b) eddy diffusion rates, a function of concentration difference in adjacent gridboxes for a particular specie. Recall that the meridional circulation, i.e. process (a), tended to weaken for both the 2100 ocean run and the 2100 all changes run. Also, the increase in ozone in the troposphere by 2100 would tend to weaken the downward diffusional flux of ozone, i.e. process (b), from the stratosphere to the troposphere. Both these factors together would tend to decrease the advective term in the region of descent. However, Table 7 implied little change – evidently such processes impacted ozone only to a minor extent in the model. In the region of ascent, a weaker (a) would tend to increase ozone (less transported upwards) whereas a weaker (b) would tend to decrease ozone (weaker downward diffusional flux due to higher ozone in the troposphere). Table 7 implied that process (b) was the more important. For NO_x the 2100 ocean run chemical loss increased significantly consistent with the faster chemical removal of NO_x in the damper, warmer atmosphere. For the advective terms, in the region of ascent the same result held for NO_x as for Ox. In the region of descent, however, the opposite was true i.e. despite a weakening in (a) and (b), the advective term increased for the all 2100 changes run. Here, NO_x increased to such an extent in the troposphere that the vertical gradient at the tropopause was sometimes actually negative with height (though the stratospheric abundance, which is fixed here, may increase in the real world as nitrous oxide emissions grow). Then, the upward diffusional flux coupled with the slower meridional circulation led to an overall increase in the advective contribution. However, this increase was small in comparison with the increase in the chemical sinks. Naturally it would be interesting to repeat this diagnosis using a model with better vertical resolution, a higher lid and interactive stratospheric chemistry.

4.10.1 Future/past response of the Hadley/Ferrel cells

Grenfell et al. (2001) have used the same model to investigate chemistry-climate interaction occurring from the pre-industrial (PI) era (1850) to the present (2000). Those authors calculated broadly comparable results to other, similar studies in the literature. However, they noted a strengthening of the meridional circulation from 1850 to 2000, whereas the present work has suggested a weakening from 2000 to 2100. The PI response was attributed to warmer SSTs leading to large increases in (absolute) water vapor in the lower troposphere. Enhanced radiative heating then resulted in decreased dynamical stability in the lower troposphere which strengthened the upward branch of the Hadley cell. But such an effect also occurred in the runs analyzed here, so the situation must be more complex. A possible explanation is the differing ozone and water distributions. An important caveat here is, due to the fixed SSTs in the model these substances could only affect the temperature away from the surface. When considering changes in heating rate it is preferable to examine % ozone (and water) change rather than the absolute change. Figurs 5a and b show the % ozone change since PI in January and July; Figs. 5c and d show the same quantity but from 2000 to 2100, for the 2100 all changes run. In July, industrialization (Fig. 5b) led to largest %ozone increases in the NH lower troposphere at around 55N. This

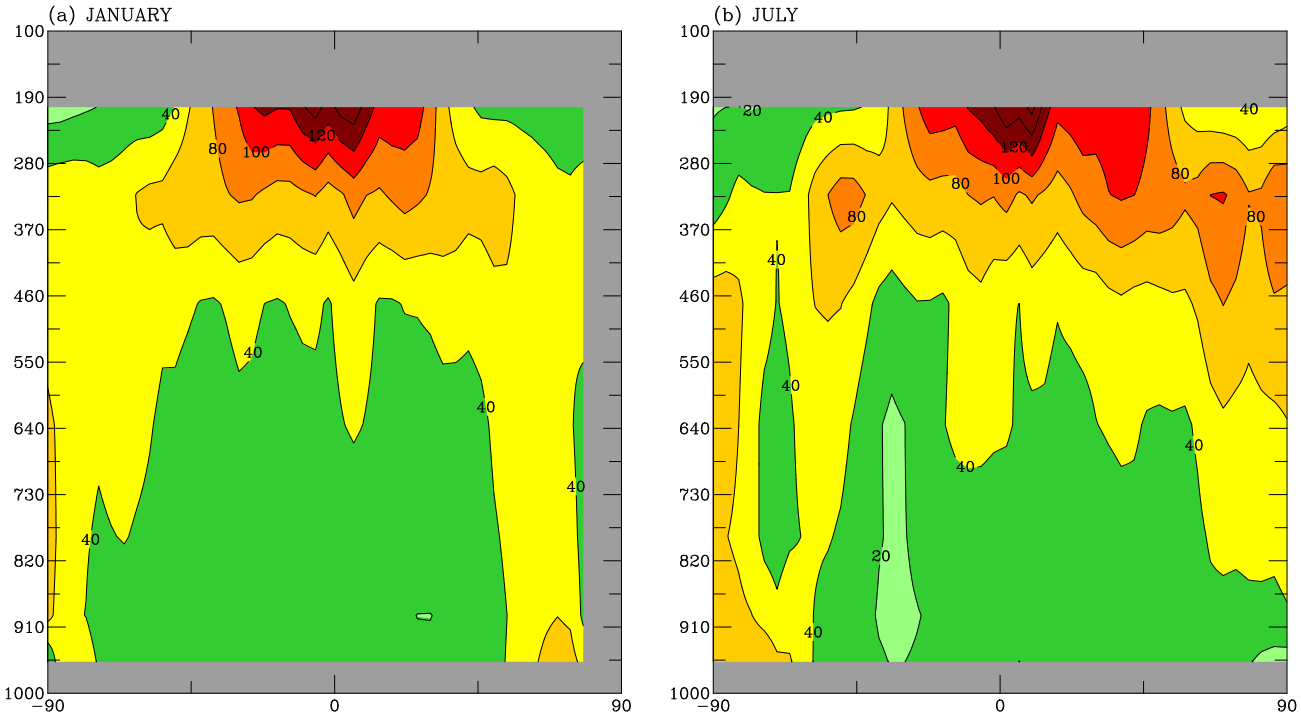

Fig. 6. %Water change in **(a)** January, **(b)** July for the all changes run – control run.

favored heating below the ascending branch of the Ferrel cell hence tended to strengthen the meridional circulation. In July, the all 2100 changes run, with its very different emissions scenario, led to %ozone increases mainly in tropical regions which peaked at the ground and at 300 mb. The lower peak tended to strengthen, whereas the upper peak tended to weaken the upward branch of the Hadley cell. Figures 6a and b show %water vapor change for the all 2100 changes run in January and July. The %peak occurred in the tropical upper troposphere and extended over both Hadley and Ferrel cells. The PI %water response (not shown), was similar except more confined in latitude (from 5 N to 5 S), which also tended simultaneously to weaken the ascending Hadley branch and strengthen the descending branch. In summary, results suggested that the ozone rather than the water changes were responsible for the differing behavior for the PI, compared with the 2100 runs. The water changes tended to strengthen and weaken alternate branches of the circulation in both sets of runs whereas the ozone changes tended to favour a strengthening in the circulation from 1850 to 2000 and a weakening from 2000 to 2100. Again, we stress that the impact may be quite different when SSTs are allowed to respond to the chemical changes.

5 Conclusions and future work

Our results imply that the major contributors to anthropogenic ozone production over the coming century will be NO_x fossil fuel and methane increases. The run with all 2100 changes suggested a July increase of 41.1% for ozone and 11.8% for OH. The extra ozone occurred mainly in the tropics and extra-tropics where most levels featured an increase of 100–130%. OH was enhanced most (by 20–60%, especially in the tropics) due to NO_x increases from 2100 fossil fuels and to a lesser extent due to increases in lightning and aircraft emissions. Roughly two-thirds of this increase was offset by decreases arising from increases in methane and to a lesser extent industrial CO and NMHCs. Although global mean OH decreased in these runs, OH was consistently increased in the NH upper troposphere in summer. This was possibly related to especially high ozone (see Sect. 4.4 for further details). Changing the ocean from 2000 to 2100 conditions led to generally higher ozone in our model compared with other studies which investigated the effect of temperature and relative humidity changes. A possible explanation for this is, we included NO_x increases due to lightning changes. To our knowledge, this effect is not accounted for in other studies (except for the recent Johnson et al., 2001 study).

The model has compared well with Ox_Comp results in two regards. Firstly, the response of OH to a 10% increase

in methane yielded a 2.9% decrease for our model compared with a decrease in the range 2.9 to 3.5% for the Ox_Comp models. Secondly, our all 2100 changes run produced a 15.8 DU mean increase in the tropospheric ozone burden, compared with 14.7–16.5 DU for the other Ox_Comp models.

Results are obviously sensitive to the emissions scenario. The A2p scenario employed the highest emissions of the four IPCC marker scenarios. Our runs did not include increases in SO_2 (hence sulfate aerosol) and NH_3 specified by A2p. The magnitude and distribution of future isoprene and other NMHC emissions are generally uncertain and were accounted for indirectly by estimating an equivalent CO burden increase. Also, the direct radiative impact of increased CO did not feature in our radiative calculations, although this is likely to be small (Ramanathan et al., 1987). Future work should address these uncertainties.

It is interesting to dicuss how our results would change had we analyzed only one year (as in the TAR study). Global mean ozone and OH did not change greatly from year to year (varying from 401 to 403 Tg and from 5.5 to 5.6×10^5 molecules/cm^3 in January respectively). Rather more internal variability was evident however, on moving to a single level. On the lowermost level (centered at 959 hPa) January zonal ozone varied year-to-year from 36 to 40 ppbv in the NH (2-sigma NH-mean=2.7 ppbv) and from 20 to 22 ppbv in the SH (2-sigma SH-mean =1.7 ppbv). For OH in January, the lowermost level featured 6.45 (2-sigma NH-mean=0.1)$\times10^5$ molecules/cm^3. On moving to zonal bands, the variability increased significantly, e.g. at 2°N, January OH mean=11.15, (2-sigma=0.66)$\times10^5$ molecules/cm^3, and at a single location would be commensurately greater. Previous tests with earlier versions of the GISS model without interactive chemistry have suggested that the atmospheric variability increases by up to an order of magnitude when the ocean is allowed to respond.

What impact could our crude stratosphere have on the results? Estimating this is difficult because the Brewer-Dobson (BD) circulation may strengthen or weaken in response to GHG forcing depending on subtle changes in the refractive index and amplitude of planetary waves (PWs). There exist complex feedbacks between wave activity, temperature and ozone loss at high latitudes. A weakened BD circulation, for example (with less PW forcing) would imply less stratospheric-tropospheric exchange hence less downward transport of ozone and NO_x.

Comparing this work with Grenfell et al. (2001), which investigated changes since the pre-industrial (PI) era, has suggested that the meridional circulation in the troposphere may strengthen or weaken depending on the water vapor and ozone responses. An increase in ozone (a heating source) occurring at the bottom of a rising Hadley branch, for example, will tend to strengthen, whereas an ozone increase occurring at the top of the branch will tend to weaken the circulation. The Ox_Comp study showed considerable differences in the peak height, and latitude of the ozone response. The NH PI ozone response (which led to a stronger circulation) calculated by Grenfell et al. (2001) tended to occur poleward of the 2100 response (which led to a weaker circulation) due to the differing emissions scenarios.

Acknowledgement. The authors thank D. Koch for providing the sulfate data, O. Wild and M. Prather for providing the original fastj photolysis code, J. Lerner for providing the 2100 ocean, R. Rudy for useful advice and D. Rind for helpful discussion. We thank N. Savage for referee comments and T. Karl for a short comment. This work was funded under NASA's Atmospheric Chemistry Modeling and Analysis Program, NASA NCC5-328 and EOS NCC 5-270.

References

Baughcum, S. L., Tritz, T. G., Henderson, S. C., and Pickett, D. C.: Scheduled Civil Aircraft Emission Inventories for 1992: Database development and Analysis, NASA CR-4700, 1996.

Bengtsson, L., Botzet, M., and Esch, M.: Will greenhouse gas-induced warming over the next 50 years lead to higher frequency and greater intensity hurricanes?, Tellus, 48A, 57–73, 1996.

Brasseur, G. P., Kiehl, J. T., Muller, J. F., Schneider, T., Granier, C., Tie, X. X., and Hauglustaine, D.: Past and future changes in global tropospheric ozone and climate: impact on radiative forcing, Geophys. Res. Lett., 25, 3807–3810, 1998.

Collins, W. J., Derwent, R. G., Johnson, C. E., and Stevenson, D. S.: The impact of human activities on the photochemical production and destruction of tropospheric ozone, Quart. J. Roy. Met. Soc., Part A, 126, 566, 1925–1951, 2000.

Del Genio, A. D. and Yao, M. S.: A prognostic cloud water parameterization for global climate models: The GISS scheme, Am. Meteorol. Soc. Monogr., 46, 181–184, 1993.

Del Genio, A. D., Yao, M. S., Kovarl, W., and Lo, K. K. W.: A prognostic cloud water parameterization for global climate models, J. Clim., 9, 2, 270–304, 1996.

Dentener, F. J. and Crutzen, P. J.: Reaction of N_2O_5 on tropospheric aerosols: Impact on the global distributions of NO_x, O_3, and OH, J. Geophys. Res., 98, 7149–7163, 1993.

Grenfell, J. L., Shindell, D. T., Koch, D., and Rind, D.: Chemistry-climate interactions in the Goddard Institute general circulation model. 2. New insights into modeling the pre-industrial atmosphere, J. Geophys. Res., 106, 33 435–33 451, 2001.

Grewe, V., Brunner, D., Dameris, M., Grenfell, J. L., Hein, R., Shindell, D., and Staehelin, J.: Origin and variability of upper tropospheric nitrogen oxides and ozone at northern mid-latitudes, Atmos. Environ., Part B, 53, 1–19, 2001a.

Grewe, V. M., Dameris, M., Hein, R., Sausen, R., and Steil, B.: Future changes in the atmospheric composition and the impact of climate change, Tellus, Ser. B, 53, 103–121, 2001b.

Hauglustaine, D. D., Brasseur, G. P., Walters, P. J., Rasch, J.-F., Muller, L. K., Emmons, and Carroll, M. A.: MOZART, a global chemical transport model for ozone and related chemical tracers 2. Model results and evaluation, J. Geophys. Res., 103, 28 291–28 335, 1998.

Hansen, J., Russell G., Rind, D., Stone P., Lacis, A., et al.: Efficient three-dimensional global models for climate studies: models I and II, Mon. Weather Rev., 111, 609–662, 1983.

Hansen, J., Sato, M., Ruedy, R., Lacis, A., Asamoah, K., et al.: Forcings and chaos in interannual to decadal climate change, J. Geophys. Res., 102, 25 679–25 720, 1997.

IPCC (Intergovernmental Panel on Climate Change): Climate change 1995: the science of climate change, edited by J. T. Houghton, Meira Filho, L. G., Callander, B. A., Harris, N., Kattenberg, A., et al., Cambridge University Press, Cambridge UK, 1996.

IPCC (Intergovernmental Panel on Climate Change): Climate Change 2001: the scientific basis, contribution of working group 1 to the third assessment report (TAR) of the intergovernmental panel on climate change, Houghton, J. T., Ding, Y., Griggs, D. J., Noguer, M., van der Linden, P. J., et al. (Eds), Cambridge University Press, UK and New York, NY, USA, 881, 2001.

Jaegle, L., D. Jacob, J., Brune W. H., Faloona, I. C., Tan, D., et al.: Ozone production in the upper troposphere and the influence of aircraft during SONEX: Approach of NO(x)-saturated conditions, Geophys., Res. Lett., 26, 3081–3084, 1999.

Johnson, C. E., Collins, W. J., Stevenson, D. S., and Derwent, R. G.: The relative roles of climate and emissions changes on future oxidant concentrations, J. Geophys. Res., 104, 18 631–18 645, 1999.

Johnson, C. E., Stevenson D. S., Collins, W. J., and Derwent R. G.: Role of climate feedback on methane and ozone studied with a coupled Ocean-Atmosphere-Chemistry model, Geophys. Res. Lett., 28, 1723–1726, 2001.

Kato, N., and Akimoto, H.: Anthropogenic emissions of SO_2 and NO_x in Asia: Emissions inventories, Atmos. Environ., 26A, 2997–3017, 1992.

Koch, D., Jacob, D., Tegen, I., Rind, D., and Chin, M.: Tropospheric sulfur simulation and sulfate direct radiative forcing in the Goddard Institute for Space Studies general circulation model, J. Geophys. Res., 104, 23 799–23 822, 1999.

Lawrence, M. G., Joeckel, P., and von Kuhlmann R.: What does the global mean OH concentration tell us? Atmos. Chem. Phys. Disc., 1, 43–75, 2001.

Mickley, L., Murti, P. P., Jacob, D. J., Logan, J. A., Koch, D., et al.: Radiative forcing from tropospheric ozone calculated with a unified chemistry-climate model, J. Geophys. Res., 104, 30 153–30 172, 1999.

Poetzsch-Heffter, C., Liu, Q., Ruprecht, E., and Simmer, C: Effect of cloud types on the Earth radiation budget calculated with the ISCCP C1 dataset: methodology and initial results, J. Clim., 8, 4, 829–843, 1995.

Poppe, D., Zimmerman, J., Bauer, R., Brauers, T., Bruning, D., et al.: Comparison of measured OH concentrations with model calculations, J. Geophys. Res., 99, 16 633–16 642, 1994.

Prather, M., Gauss, M., Berntsen, T., Isaksen, I., Sunder, J., et al.: Fresh Air in the 21st Century?, Geophys., Res. Lett., 30, 2, 721–724, 2003.

Price, C., Penner, J., and Prather M.: NO_x from lightning. 1. Global distribution based on lightning physics, J. Geophys. Res., 102, 5929–5941, 1997.

Prinn, R. G., Weiss, R. F., Miller, B. R., Huang, J., Alyea F. N., et al.: Atmospheric trends and lifetime of CH_3CCl_3 and global OH concentrations, Science, 269, 187–192, 1995.

Ramanathan, V., Callis L., Cess R., Hansen J., Isaksen, et al.: Climate-chemical interactions and effects of changing Atmospheric trace gases, Rev. Geophys., 25, 1441–1482, 1987.

Ramstein, G., Serafini-Le Treut Y., Le Treut, H., Forichon, M., and Joussaume S.: Cloud processes associated with past and future climate changes, Clim., Dynam., 14, 233–247, 1998.

Rind, D.: Latitudinal temperature gradients and climate change, J. Geophys. Res., 103, 5943–5971, 1998.

Roelofs, G. J. and Lelieveld J.: Tropospheric ozone simulation with a chemistry-general circulation model: Influence of higher hydrocarbon chemistry, J. Geophys. Res., 105, D18, 22 697–22 712, 2000.

Russell, G. L., Miller, J. R., and Tsang, L. C.: Seasonal oceanic heat transports computed from an atmospheric model, Dyn. Atm. Oceans, 9, 253–271, 1985.

Shindell, D. T., Grenfell, J. L., Rind, D., Price, C., and Grewe, V.: Chemistry-climate interactions in the Goddard Institute for Space Studies general circulation model 1. Tropospheric chemistry model description and evaluation, J. Geophys. Res., 106, D8, 8047–8075, 2001.

Stevenson, D. S., Johnson, C. E., Collins, W. J., and Derwent., R. G., and Edwards, J. M.: Future estimates of tropospheric ozone radiative forcing and methane turnover – the impact of climate change, Geophys. Res. Lett., 27, 2073–2076, 2000.

Trainer, M., Parrish, D. D., and Buhr, M. P.: Correlation of ozone with NO_y in photochemically aged air, J. Geophys. Res., 98, 2917–2932, 1993.

Wang, Y., Jacob, D. J., and Logan, J. A.: Global simulation of tropospheric O_3-NO_x-hydrocarbon chemistry. 1. Model formulation. J. Geophys. Res., 103, 10 713–10 725, 1998.

Wild, O., Zhu, X., and Prather, M. J.: Fast-J: Accurate simulation of in- and below-cloud photolysis in tropospheric chemical models, J. Atm. Chem., 37, 3, 245–282, 2000